npj | 2D Materials and Applications

www.nature.com/npj2dmaterials

ARTICLE OPEN

Hybrid graphene tunneling photoconductor with interface engineering towards fast photoresponse and high responsivity

Li Tao[1], Zefeng Chen[1], Xinming Li[1], Keyou Yan[1] and Jian-Bin Xu[1]

Hybrid graphene photoconductor/phototransistor has achieved giant photoresponsivity, but its response speed dramatically degrades as the expense due to the long lifetime of trapped interfacial carriers. In this work, by intercalating a large-area atomically thin MoS_2 film into a hybrid graphene photoconductor, we have developed a prototype tunneling photoconductor, which exhibits a record-fast response (rising time ~17 ns) and a high responsivity (~3×10^4 A/W at 635 nm illumination with 16.8 nW power) across the broad spectral range. We demonstrate that the photo-excited carriers generated in silicon are transferred into graphene through a tunneling process rather than carrier drift. The atomically thin MoS_2 film not only serves as tunneling layer but also passivates surface states, which in combination delivers a superior response speed (~3 orders of magnitude improved than a device without MoS_2 layer), while the responsivity remains high. This intriguing tunneling photoconductor integrates both fast response and high responsivity and thus has significant potential in practical applications of optoelectronic devices.

npj 2D Materials and Applications (2017)1:19 ; doi:10.1038/s41699-017-0016-4

INTRODUCTION

Photodetectors with high speed and responsivity are of crucial importance for optoelectronic applications. Benefiting from their large surface area and unique electronic properties, two-dimensional (2D) materials are promising building blocks in optoelectronic devices.[1, 2] The gapless semi-metallic band structure of graphene gives rise to its high mobility, extremely broad optical absorption and ultrafast carrier dynamics,[3–6] making this emerging 2D material particularly attractive in photodetection applications.[7, 8] However, the responsivity of phototransistor comprised of pristine graphene is limited to the level of mA/W due to the low optical absorption rate and fast carrier recombination in graphene.[8, 9]

Recently researchers have proposed an effective method to improve the responsivity of graphene-based photodetector by adding a light absorption material, such as PbS quantum dots,[10] Bi_2Te_3,[11] perovskites,[12, 13] silicon (Si),[14, 15] carbon nanotubes,[16] atomically thin MoS_2,[17, 18] and organic crystal,[19] as active layer and mainly remaining the graphene as the channel transport layer. This hybrid graphene photoconductor/phototransistor introduces a vertical built-in field at the interface for exciton dissociation. The photo-excited carriers in the active layer can be efficiently transferred into graphene, of which the electrical conductance is highly sensitive to external carrier injection.[20] Although this device configuration brings great enhancement of responsivity, the response speed of graphene-based photoconductor drastically degrades as the cost. The interface trap states, together with the drift time of photo-excited carriers in the depletion region, increase the response time into the range from several microseconds to several seconds.[10–19] This trade-off between response speed and responsivity makes it a great challenge to achieve fast and high-gain photoresponse simultaneously in graphene-based photodetectors, severely limiting their potential application for photodetection.

Interface passivation has been demonstrated to improve the performance of diode photodetector,[21–23] solar cell,[24–26] and tunneling filed-effect transistor (TFET),[27, 28] but has rarely been proved in a conductive mode photodetector, i.e., a photoconductor/phototransistor. Here, we propose a high-performance atomically thin hybrid graphene tunneling photoconductor constructed with light absorption and interface passivation layers. This hybrid graphene photoconductor exhibits a response time of ~17 ns, which is improved by ~3 orders of magnitude compared with the device without MoS_2 intercalation and is at present the shortest one among those of hybrid graphene photoconductors/phototransistors, along with a high responsivity across a broadband spectral range (~3×10^4 A/W at 635 nm illumination with 16.8 nW power). In our device, the Si serves as an optically active layer and MoS_2 film acts as a passivation layer for reducing surface states, suppressing carrier recombination at the interface, and offering an ultra-thin layer for the carrier tunneling. Carrier transfer process driven by ultra-fast quantum tunneling effect rather than by the carrier drift in the depletion region enables a superior response speed, while the responsivity remains high as a major merit of hybrid graphene photoconductor/phototransistor. The device designs and results not only provide a unique structure for better understanding the photocarrier transfer and transport processes in 2D-layered nanomaterials but also pave the way for the development of state-of-the-art graphene-based photodetector with both high speed and responsivity for practical applications.

RESULTS AND DISCUSSION

Device structure

Figure 1a schematically shows the structure of the hybrid graphene photoconductor, and Fig. 1b presents the top view optical image of a typical device. A moderately *n*-doped silicon (n-Si, carrier density ~10^{15} cm^{-3}) wafer was used as the starting

[1]Department of Electronic Engineering, The Chinese University of Hong Kong, Shatin, NT, Hong Kong SAR, China
Correspondence: Xinming Li (xmli1015@gmail.com) or Jian-Bin Xu (jbxu@ee.cuhk.edu.hk)

Received: 5 December 2016 Revised: 23 May 2017 Accepted: 30 May 2017
Published online: 03 July 2017

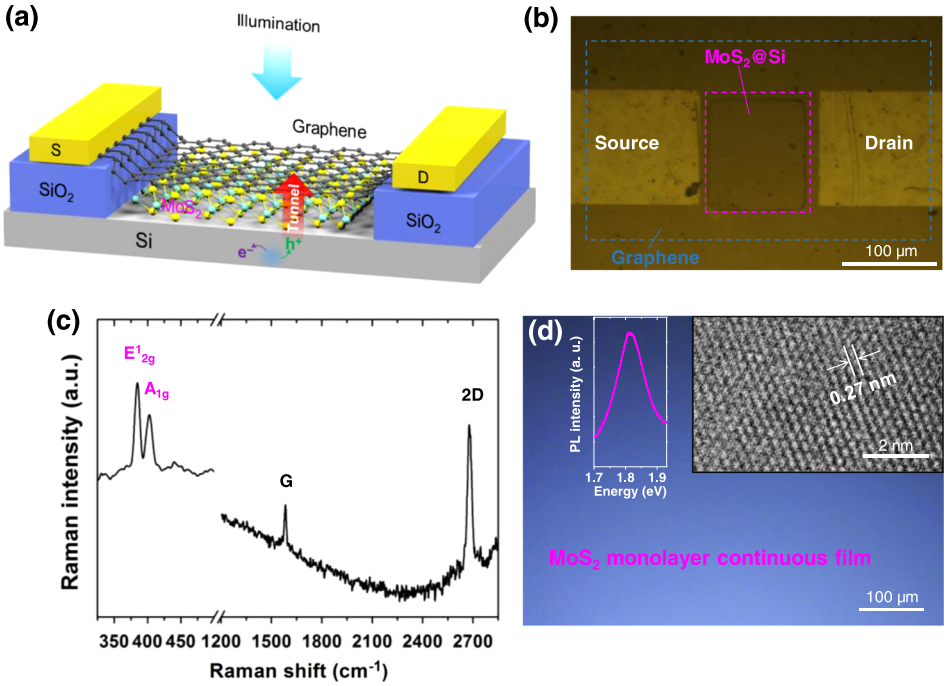

Fig. 1 Schematic diagram and characterizations of the hybrid graphene photoconductor. **a** Schematic and **b** *top view* optical image of the device. **c** Raman spectra taken in the area within the *violet dashed rectangle* in (**b**). **d** Optical image of monolayer MoS_2 film before transfer. *Upper left inset*: a typical PL spectrum of monolayer MoS_2 film with the peak at 1.82 eV. *Upper right inset*: HRTEM image of the MoS_2 film

substrate. A 100 nm SiO_2 thin layer was grown on the Si wafer and a 105 × 115 μm Si window was defined by CF_4 etching. Afterward, monolayer MoS_2 film grown by chemical vapor deposition (CVD) was transferred onto the Si groove region of the substrate, and a subsequent pattern process was carried out to enable the remaining MoS_2 cover the Si window. After monolayer graphene film was transferred onto the MoS_2/Si heterostructure, a pair of Au source/drain electrodes was thermally deposited atop graphene to form a channel with 125 μm in length. Figure 1c displays the Raman spectra taken in the vertical heterostructure area of the device (violet dashed rectangle in Fig. 1b). Characteristic Raman signals of both MoS_2 and graphene were clearly detected. The feature peaks of MoS_2 at 384.6 cm^{-1} (E^1_{2g}) and 403.1 cm^{-1} (A_{1g}) with an 18.5 cm^{-1} difference indicate the monolayer nature of the MoS_2 film.[29] The high quality of monolayer graphene was also confirmed by the absence of D-band and the high intensity ratio of 2D and G peaks.[30] Figure 1d shows a typical optical image of large-scale continuous monolayer MoS_2 film before transfer. Photoluminescence measurement of the MoS_2 film (*upper left inset* of Fig. 1d) reveals a direct optical bandgap of 1.82 eV, which reconfirms its monolayer feature.[31] High-resolution transmission electron microscopy (HRTEM) image in the upper right inset of Fig. 1d presents a highly crystalline structure of monolayer MoS_2.

Photoresponse performance

Figure 2 provides the photoresponse characteristics of the hybrid graphene photoconductor. Typical illumination power-dependent response at a wavelength of 635 nm has been measured, as shown in Fig. 2a. The device shows negative photoresponses because photo-excited holes are injected into n-type graphene while electrons are trapped in Si, lowering graphene's quasi-Fermi level through photo-gating effects.[10, 14, 32] Both MoS_2 and n-Si can bring n-dopants to graphene (see Supplementary Information S1),[14, 18, 33] thus the Fermi level of graphene prior to being illuminated is above its Dirac point. The work function of graphene in the channel area is measured to be ~4.4 eV with a Kelvin probe force microscopy (KPFM) system (Figure S1b). The photocurrent I_{ph}, which is defined as the absolute difference between light current I_{light} and dark current I_{dark} ($I_{ph} = |I_{light} - I_{dark}|$), shows a monotonic increase as the light power P increases. The responsivity, together with the photocurrent as functions of illumination power at $V_d = 5$V are given in Fig. 2b. The photoconductor shows a considerably high responsivity of $\sim 3 \times 10^4$ A W^{-1} at the light power of 16.8 nW, which far exceeds that in pure graphene device, and has the same order as that in graphene/Si photoconductor without MoS_2 intercalation (see Supplementary Information S2). As the responsivity increases with decreasing light power, a higher responsivity is expected in ultra-weak illumination. The corresponding photoconductive gain G is calculated to be $\sim 5.8 \times 10^4$ by using the relation $G = (I_{ph}/q)/(P/hv)$, where q is the elementary charge, h is the Plank constant and v is the frequency of incident light. Such an outstanding gain reveals that the photo-excited carriers can travel through the graphene channel for numerous times before recombination according to the definition of gain $G = \tau_{lifetime}/\tau_{tr}$, where $\tau_{lifetime}$ is the lifetime of injected carriers from Si and τ_{tr} is the carrier transit time across the channel.[34] The trapped photo-excited electrons in Si enable the excess hole conservation (with long $\tau_{lifetime}$) in graphene by capacitive coupling, leading to the carrier reinvestment in graphene channel and the ultrahigh gain in the photodetector.[10, 14, 35]

Wavelength-dependent photoresponses at 5 V bias were measured via quartz tungsten halogen lamp filtered with a monochromator. Normalized photocurrent vs. light wavelength plotted in Fig. 2c reveals a broad spectral response with considerable responsivity from visible light to the near-infrared region (~1120 nm). Relatively higher photoresponse than pure Si photodetector from violet to green is assigned to additional absorption by monolayer MoS_2.

Transient performance

Temporal response of the hybrid graphene photoconductor was conducted under electrically modulated 635 nm light pulse having illumination power of 3.35 μW. Figure 3a shows the transient characteristics of the device at repeated frequency of 2 Hz, which

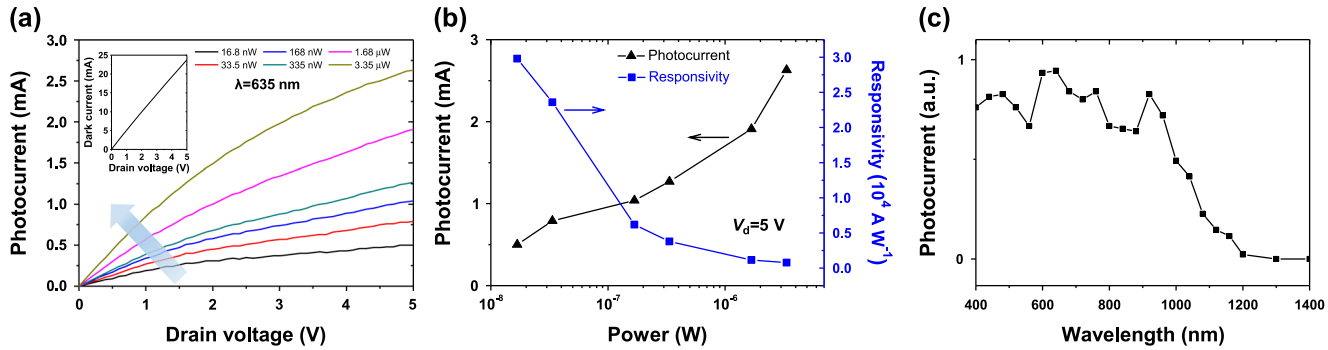

Fig. 2 Photoresponse of the hybrid graphene photoconductor. **a** Photocurrent vs. drain voltage under various light powers at 635 nm wavelength. The *arrow* indicates the direction of light power increase. The *inset* shows the dark current of the device. **b** Power-dependent photocurrent and photoresponsivity at 5 V drain voltage calculated from the data in (**a**). **c** Normalized photocurrent vs. illumination wavelength

demonstrates highly repeatable and stable switching characteristics between light-off and light-on states. When the repeated frequency of light input increases to 100 kHz, the photoconductor can maintain its promising switching performance (Fig. 3b). The fast rising edge followed by the quick falling tail in the light-switching-on front results from a competition between hole drifting and electron diffusion processes in the depletion region.[15] The spikes in light switching points are due to the limitation of the pulse generator.

In order to further investigate the response speed of the device, which reveals the capacity to follow high-frequency optical signals, the detailed information of the rising and falling edges in a single switching cycle is provided in Fig. 3c, d, respectively. An ultra-fast response is found with the rising time (response time) τ_{rise} of ~17 ns and falling time (decay time) τ_{fall} of ~1.1 μs by fitting the rising and falling edges using exponential equations $I_{ph} = I_{OFF}\left(1 + A\exp\left(-\frac{t}{\tau_{rise}}\right)\right)$ and $I_{ph} = I_{ON}\left(1 - B\exp\left(-\frac{t}{\tau_{fall}}\right)\right)$, respectively, where I_{OFF}, I_{ON}, A and B are fitting parameters. In contrast to the graphene/Si photoconductor without MoS_2 layer intercalation which gives a response time of 12 μs (inset in Fig. 3c), this hybrid graphene photoconductor with MoS_2 interface layer greatly enhances the response speed by ~3 orders of magnitude. Transient response measurements under infrared light (905 nm) were also performed (see Supplementary Information S3), from which similar fast response (τ_{rise} ~35 ns) can be identified. Note that some oscillation signals with a period of ~28 ns occur at the rising and falling edges; it is suggested to be the intrinsic RC oscillation of the operating circuit. By measuring the resistance R and capacitance C of the operating circuit (graphene channel) ($2.3 \times 10^2 \Omega$ and 2.1×10^{-11}F, respectively), we obtain the calculated RC time constant $T_{RC} = 2\pi RC \approx 30$ ns, which is self-consistent with the directly measured value from the oscilloscope. The phenomenal response speed of the tunneling graphene-based photoconductor far exceeds those in previous reports on hybrid graphene photoconductors/phototransistors, and is even close to the limitation of intrinsic circuit oscillation. Furthermore, in stark contrast to commercial Si photoconductors/phototransistors of which response times are around several tens of microseconds (e.g., OP602TX Si phototransistor from OPTECK with τ_{rise}~20 μs),[36] this hybrid graphene photoconductor overcomes the limitation of pure Si device by enhancing the response speed of about 3 orders. This results from the photo-excited carriers in our device transiting across the graphene channel, which is a much faster process than the carriers transiting across the Si channel in pure Si photoconductors. Such fast photoresponse makes this device highly promising in high-frequency optical sensing applications such as military warning, high-speed imaging and chemical sensing.

Photocarrier tunneling and interface passivation

We have proposed a synergistic mechanism to explain the extraordinary performance of the hybrid graphene photoconductor with the MoS_2 interface layer, which will be demonstrated in the following. Figure 4a illustrates the band diagram of the device. A Schottky barrier is formed at the interface between graphene and Si. Electron and hole pairs (EHPs) are generated in the depletion region under illumination. The excess holes in n-Si result in a small hole quasi-Fermi level difference between graphene and Si (ΔE_{Fp}), acting as the driving force for hole transport.[25, 37] The built-in field separates the EHPs and consequently the holes are transferred into graphene, leading to the conductance reduction of graphene. It is estimated that the quasi Fermi level of graphene is pulled down by 9.2 meV due to the photo-excited holes injection under 3.35 μW illumination and the built-in barrier height $q\varphi_{bi}$ prior to being illuminated is ~0.15 eV (see Supplementary Information S4). This Fermi level lowing caused by illumination is also detected by the Raman G peak redshift in n-type graphene with increasing laser power (Figure S4b). Here the MoS_2 film plays several crucial roles in device operating. First, MoS_2 passivates the interface of the Schottky junction to reduce trap states and to further suppress carrier recombination. Meanwhile the ultra-flat MoS_2 underneath graphene allows the intrinsic electronic properties to be retained in graphene.[38] Second, the relatively wide electronic bandgap of monolayer MoS_2 (~2.4 eV) results in a straddling gap at MoS_2/Si interface, namely, type-I heterostructure.[39, 40] In this band alignment, photo-excited holes are accumulated at the interface triangular well (*green circles* in Fig. 4a), while electrons are blocked from transiting towards graphene. The valence band offset at MoS_2/Si (ΔE_v) around 1.1 eV[39] provides a barrier to prohibit the thermionic emission for the photo-excited holes (thermal energy at 300 K is ~26 meV), thus suppressing the thermal noise. Third, the atomic thickness of MoS_2 enables the carrier wave function in Si to interact with that in graphene, causing the carrier quantum tunneling through MoS_2 layer. The band bending at MoS_2/Si interface (Fig. 4a) generates a strong built-in field that further enhances the hole tunneling.

The photo-excited carriers (holes) in the device are injected into graphene via an ultra-fast tunneling process. The response time τ_{rise} is affected by the drift time for photo-excited carriers to travel from depletion region to the Schottky junction interface (τ_{drift}), the average time for carriers to transit through interface trap states (τ_{trap}), the average time for carriers to tunnel through MoS_2 film (τ_{tunnel}) and carrier transit time in graphene channel (τ_{tr}). τ_{tr} is estimated to be $\tau_{tr} = \frac{L}{\mu_{graphene} V_d / L} \approx 10$ ns, where L is the channel length (125 μm) and $\mu_{graphene}$ is carrier mobility in graphene which has been derived to be ~3.1×10^3 cm^2 V^{-1} s^{-1} (see Supplementary Information S4). τ_{trap} is greatly lessen with MoS_2 passivation, as

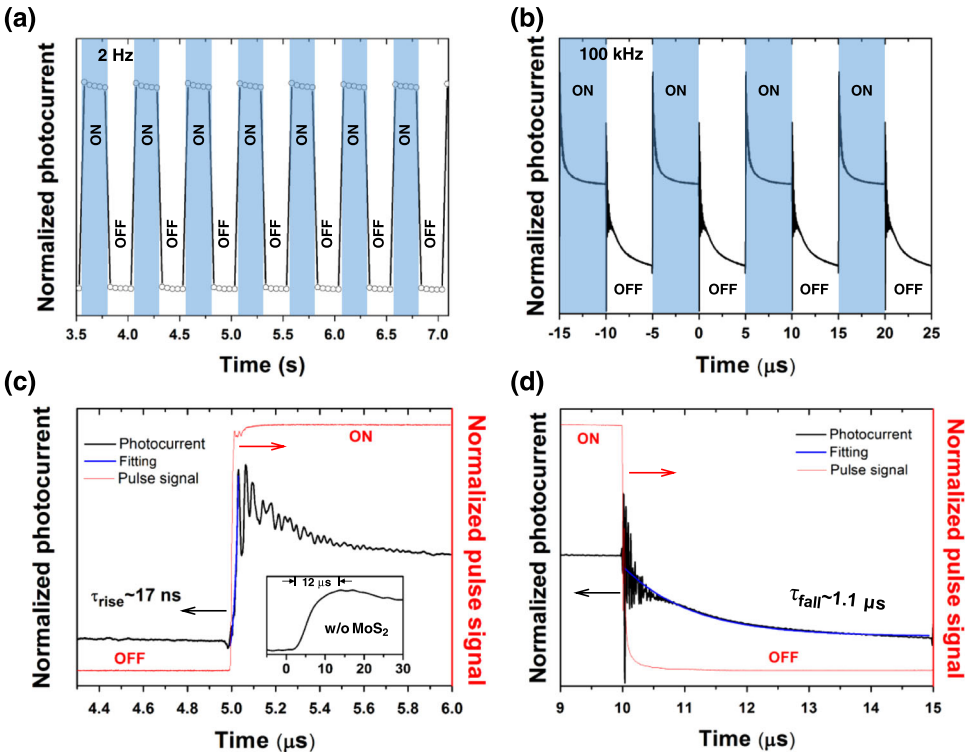

Fig. 3 The temporal performance of the hybrid graphene photoconductor. Switching characteristics of the device under **a** 2 Hz and **b** 100 kHz square-wave light pulse (635 nm). Enlarged views of (**b**) at light being switched on (**c**) and light being switched off (**d**). *Inset* in (**c**): rising edge of the device without MoS_2 layer intercalation

discussed above. τ_{drift} is also reduced when MoS_2 layer is used since MoS_2 shares the depletion region of the Schottky junction and makes the length of remaining depletion region in Si shorter. τ_{tunnel} is highly sensitive to the tunneling barrier (MoS_2 film) thickness d, which is written as below based on the Wentzel–Kramers–Brillouin approximation:[34, 41]

$$\tau_{tunnel} \propto 1/T_{tunnel} \propto \exp\left[2d\sqrt{\left(\frac{8\pi^2 m_p^*}{h^2}\right)q\phi_{tunnel}}\right], \quad (1)$$

where T_{tunnel} is the carrier tunneling probability, m_p^* is the effective mass of the accumulated hole in Si, and $q\varphi_{tunnel}$ is the average barrier height for tunneling. The carrier tunneling phenomenon originates from the wave nature of carriers in quantum mechanics, and the tunneling time τ_{tunnel} is not determined by the classic transit time process (i.e., $\tau = d/v$, where v is the carrier velocity).[34] Tunneling time can be very short when the tunneling barrier is ultrathin (<2 nm), typically in the timescale of subnanosecond.[41] The high speed response in the photoconductor benefits dominantly from this ultra-fast tunneling process when the MoS_2 layer is thin enough. Additionally, graphene based Schottky junction enables the tunneling effect to occur in relatively small built-in barrier while conventional TFETs require a gate voltage for band-to-band tunneling.[28]

To certify the tunneling mechanism described above, we investigate the thickness effect of the MoS_2 passivation layer on the photoconductor performance. Figure 4b depicts the energy-band diagram of the hybrid graphene photoconductor with multilayer MoS_2 interface layer. As the tunneling barrier gets thicker, the carrier tunneling probability T_{tunnel} drastically reduces (Eq. (1)). Correspondingly, not only the tunneling time τ_{tunnel} which is inversely proportional to T_{tunnel} becomes much longer, but also the total population of photo-excited carriers which can tunnel into graphene decreases. We have fabricated control devices with multilayer MoS_2 film (~4 layers, confirmed by Raman spectrum, Figure S5a), with all the other factors unchanged. Temporal response measurements show that the photoconductor with thicker interface layer presents a response time of ~500 ns (Fig. 4c), revealing that larger tunneling barrier thickness d causes a longer τ_{tunnel} (Eq. (1)). Moreover, the photoresponsivity in the photoconductor with multilayer MoS_2 is much smaller than that of device with monolayer MoS_2 (Fig. 4d), which well agrees with the above analysis on the injected carrier population decrease (note that the increased light blocking by multilayer MoS_2 is limited).[42]

To further understand the photocarrier tunneling process, we investigate the temperature-dependent carrier transport in the device operating in diode mode (i.e., the source and drain electrodes are on graphene and Si, respectively). Figure 4e presents the photocurrent and dark current at various temperatures. Under the dark condition, the carriers have to surmount the Schottky barrier ($q\varphi_B$) for transport (*left inset* in Fig. 4e), and the dark current obeys to the traditional thermionic emission theory for Schottky diode:[34]

$$I_{dark} = AA^*T^2 \exp\left(-\frac{q\phi_B}{kT}\right)\left[\exp\left(\frac{qV}{\eta kT}\right) - 1\right], \quad (2)$$

where A is the junction area, A^* is the effective Richardson constant, T is the absolute temperature, k is the Boltzmann constant, and η is the ideality factor. The reverse saturation current at diode bias $V_{bias} = -2$V ($I_{dark,s}$) as a function of temperature is plotted in *red circles* in Fig. 4f (Arrhenius plot). A linear $\log(I_{dark,s})$ $-1/T$ dependence is found, demonstrating the carrier transport in the dark is a thermally activated process with the express $I_{dark} \propto \exp(-(E_a)/(kT))$, where E_a is the activation energy.[34] When illuminating the diode at zero bias, the current is fully contributed by photo-excited carriers ($I_{ph,0} = I_{light,0}$ at $V_{bias} = 0$), and the holes tunnel through MoS_2 layer into the graphene rather than being thermally activated (*right inset* in Fig. 4e). As illustrated in Fig. 4f, $I_{ph,0}$ at zero bias is temperature insensitive. The short-circuit hole

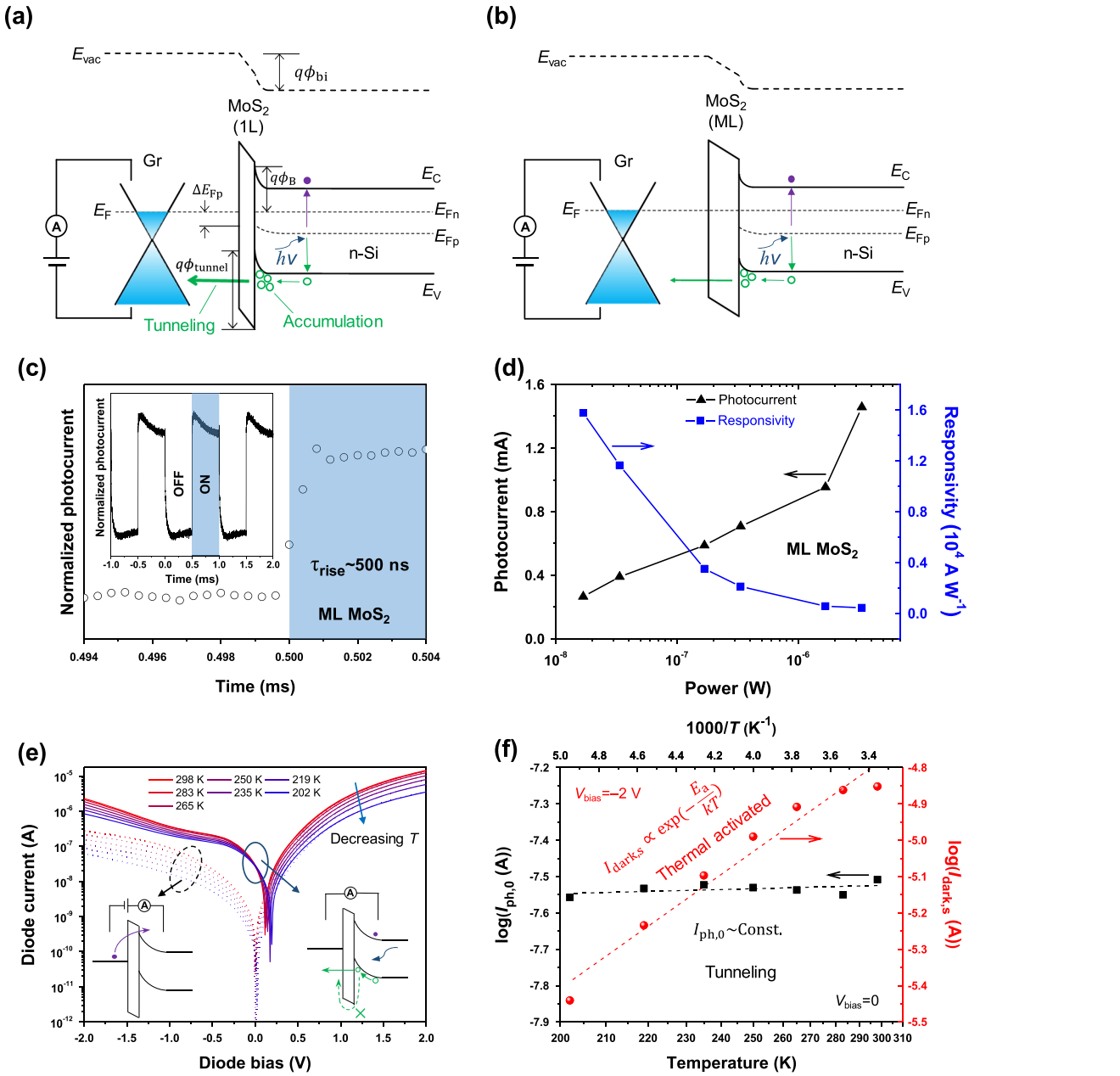

Fig. 4 Photoexcited carrier tunneling process in the hybrid graphene photoconductor. Energy-band diagram of the devices formed with monolayer (1 L) (**a**) and multilayer (ML) (**b**) MoS_2 films. The number of the *green circles* indicates the relative population of accumulated carriers. The accumulated carriers can tunnel to graphene through the MoS_2 layer, as shown by the *green lines*. The sizes of the *green lines* indicate the relative tunneling probability. A thicker tunneling barrier results in a smaller tunneling probability. **c** Transient characteristics of the hybrid graphene photoconductor with ML MoS_2 under 635 nm illumination, showing a rising time of ~500 ns. Inset is the switching performance over three periods of square-wave modulation. **d** Photocurrent and responsivity as functions of the illumination power of the device with ML MoS_2. **e** Current vs. bias curves of the device operating in diode mode in the dark (*dashed curves*) and under 635 nm (3.35 μW) illumination (*solid curves*) at various temperatures. *Insets* schematically show the carrier transport in dark (reverse bias) and under illumination (zero bias), respectively. **f** Zero-bias photocurrent ($I_{ph,0}$) and reverse saturation dark current at −2 V ($I_{dark,s}$) as functions of temperature (Arrhenius plot) extracted from (**e**). The *dashed lines* show the linear fittings

tunnel photocurrent is given by:[37]

$$I_{ph,0} = \frac{4\pi m_p^* q(kT)^2}{h^3 N_V} p_s \exp\left(-\sqrt{q\phi_{tunnel}}d\right)\left[1-\exp\left(-\frac{\Delta E_{Fp}}{kT}\right)\right], \quad (3)$$

where N_V is the effective density of states in the valence band of Si, and p_s is the concentration of holes at the interface. This expression indicates a non-thermally-activated process of the photo-excited carrier since ΔE_{Fp} promotes the carrier tunneling rather than setting up an energy barrier. From the Richardson plot of $I_{ph,0}$ ($\log(I_{ph,0}/T^2)$–$1/T$ plot) as illustrated in Figure S6, one can identify that $I_{ph,0}/T^2$ increases with decreasing temperature, which is in good coincidence with Eq. (3). The above analysis of photo-excited carrier transport at zero bias in the graphene/Si diode with MoS_2 layer can be fully applied to the device operating in photoconductor mode since there is no external vertical bias across the photoconductor (Fig. 1a).

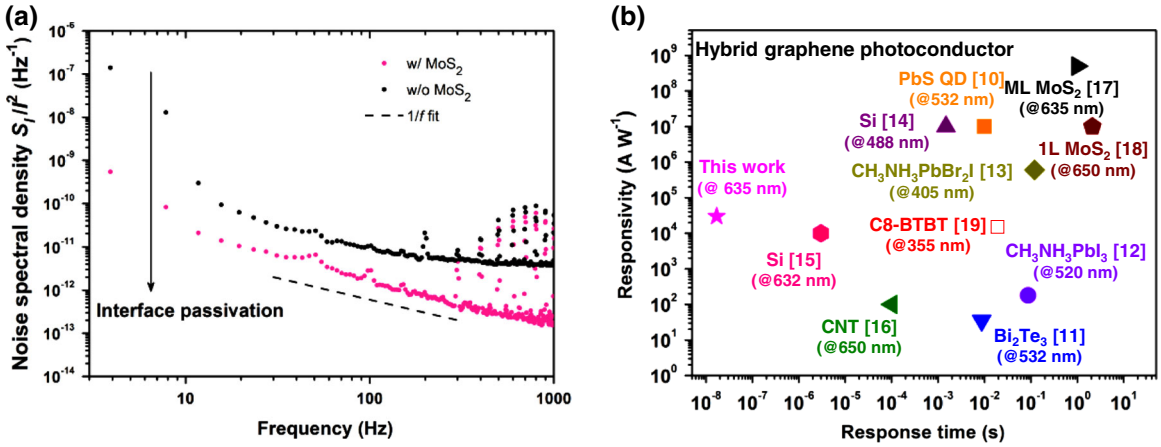

Fig. 5 **a** Normalized noise spectral density (S_I/I^2) as a function of frequency (f) for the hybrid graphene photoconductor with and without monolayer MoS_2 passivation. *Dashed line* gives the guide to eyes for 1/*f* noise. Sharp peaks at 50 Hz and its harmonics are induced by power source. **b** Comparison between response time (rising time) and responsivity of our device and those of typical reported hybrid graphene photoconductors/phototransistors, with the photoactive material adopted in the device, the corresponding reference number (in *square brackets*) and the operation wavelength (in *parentheses*) in each labeled text. *QD* quantum dot, *CNT* carbon nanotube, dioctylbenzothienobenzothiophene (C8-BTBT)

In previous studies of graphene photoconductor/phototransistor hybridized with a semiconducting active layer, the photo-excited carriers were transferred to graphene driven by the built-in field. During this process, the carriers can be trapped by interface states, thus resulting in long carrier transfer time. Here, by inserting an atomically thin MoS_2 layer into hybrid graphene photoconductor, the interface traps are passivated and thus the photo-excited carriers can be efficiently transferred into graphene through the ultra-fast tunneling process (energy-band diagram of graphene/Si junction without MoS_2 layer is shown in Figure S7). We further investigate the MoS_2 passivation effect by the noise spectra of the devices. It is widely accepted that the noise in metal-oxide-semiconductor transistors can be explained by the trap charge fluctuation mechanism.[43] The interface trap states are considered to be one of the dominant contributions to the low-frequency 1/*f* noise in monolayer graphene devices.[44–46] It is observed that the graphene-based photoconductor with MoS_2 interface layer performs more than one order of magnitude lower noise power density (S_I/I^2) when compared with the device without MoS_2 layer (Fig. 5a). The average noise amplitude A_{noise}, which is defined as $A_{noise} = \frac{1}{N}\sum_{k=1}^{N} f_k(S_I/I^2)_k$, can quantitatively probe the level of 1/*f* noise for a given frequency range.[44] For devices without and with MoS_2 passivation, A_{noise} is calculated to be 1.5×10^{-8} and 2.4×10^{-10}, respectively at low frequencies (4–191 Hz). This large noise reduction indicates that the interface traps are greatly removed by MoS_2 passivation, demonstrating that MoS_2 serves as perfect substrate for graphene.[38] By designing the graphene-based photoconductor with interface engineering, we have approached the highest response speed among hybrid graphene photoconductors/phototransistors. For detailed comparison, we have summarized the figures of merit (response time and responsivity) for some previously reported hybrid graphene photoconductors/phototransistors and our device, as shown in Fig. 5b.[10–19]

Flexible device

Furthermore, this hybrid graphene photoconductor does not require electrical gating to operate, which makes it possible to obtain flexible device if Si thin film (thickness ~200 nm) exfoliated from silicon-on-insulator is adopted (see Supplementary Information S8). Here we fabricated a flexible device on a polyimide substrate, as manifested in Figure S8a. This flexible device shows the high reliability of photoresponse under 635 nm illumination after mechanical bending for 100 times (Figures S8b, S8c). The responsivity of the flexible photoconductor under 168 nW light power is ~1×10^3 A/W, and the response time τ_{rise} is around 0.2 s. The flexible device exhibits competitive performance when comparing to previously reported flexible photodetector based on graphene[47] and other 2D materials.[48] Due to the large amount of traps in polyimide and Si thin film, the flexible device cannot response as fast as the rigid one does at present.

CONCLUSIONS

In summary, we developed an interface engineered hybrid graphene photoconductor with a record-fast response within 17 ns and a high photoresponsivity across a wide spectral band. The atomically thin MoS_2 film in the device not only passivates interface traps but also acts as a barrier for photo-excited carrier tunneling into graphene, which accounts for the remarkable response speed. We have investigated the tunneling mechanism in detail and identified the importance of incorporating tunneling barrier in atomic thickness. Temperature-insensitive short-circuit photocurrent in graphene/Si diode with MoS_2 interface layer provides strong evidence for the photo-excited carrier tunneling in the device. Also, the interface passivation by MoS_2 is demonstrated through noise analysis. This demonstrated graphene-based photoconductor with interface engineering opens a pathway towards ultra-fast, high responsivity and broadband photodetection with the large photo-active area, therefore providing a myriad of opportunities for future study and practical applications of 2D materials.

METHODS

CVD growth of MoS_2

Monolayer/few-layer MoS_2 films were fabricated using a home-built CVD system.[49] A quartz boat holding ammonium molybdate powder (6 mg) for producing uniform MoO_3 during growing was put in the center of a 2-inch CVD quartz tube. SiO_2/Si substrates treated with acetone and O_2 plasma were placed next to the boat. Another quartz boat holding precursor of S powder of 0.7 g was placed 30 cm away from ammonium molybdate. The reaction furnace was heated to 800 °C at the rate of 15 °C min^{-1} and S powder was heated to 180 °C when the reaction zone reached the temperature of 650 °C with a 50 sccm Ar flow at the pressure of ~100 Pa. After ~30 min MoS_2 growing, the furnace was cooled down to room temperature and MoS_2 films with high quality were deposited on the substrates.

Characterization

A Renishaw Spectroscope with 514.5 nm laser excitation was applied to perform Raman and PL measurements. The size of laser spot was ~1 μm. HRTEM measurements were conducted via FEI Technai F20 system. KPFM measurements were performed using a Bruker Dimension Icon system.

Photoresponse measurements

A Keithley 4200 semiconductor characterization system was applied in the measurements. Lasers with 635 and 905 nm wavelengths and a series of attenuation slices were used to generate constant illumination with various powers. A quartz tungsten halogen lamp housing (Newport 66882) combined with a monochromator was used to generate illuminations with specific wavelengths (400–1500 nm). The filtered light power is estimated to be ~2 nW at 635 nm wavelength. To make sure the lasers only illuminate the active layer area (channel) of the device, a black mask was applied to block the other region of the device. A square-wave pulse generator was used to modulate the laser to give switching illumination. An oscilloscope was connected in series with the device to investigate the switching characteristic at high-frequency optical signals. Noise analysis was conducted via a Stanford Research Systems SR760 FFT Spectrum Analyzer.

Data availability

All the data shown in this work are available from the authors.

ACKNOWLEDGEMENTS

The authors are thankful to Dr. Hui Yu for valuable advice and Mr. Guodong Zhou and Mr. Ningqi Luo for technical support. The work is in part supported by Research Grants Council of Hong Kong, particularly, via Grant Nos. N_CUHK405/12, AoE/P-02/12, 14207515, 14204616, and CUHK Group Research Scheme. X.M. Li and J. B. Xu would like to thank the National Natural Science Foundation of China for the support, particularly, via Grant Nos. 51402060 and 61229401. X.M. Li also thanks the Postdoctoral Fellowship by CUHK.

AUTHOR CONTRIBUTIONS

L.T. designed the device structure. X.M.L. and J.B.X. supervised the project. L.T. did the material synthesis and characterization. L.T. and Z.F.C. fabricated the device and performed the photoresponse measurements. L.T., Z.F.C., X.M.L., K.Y.Y. and J.B.X analyzed the data. L.T. wrote the manuscript. L.T., X.M.L., K.Y.Y. and J.B.X. revised the manuscript. All the authors discussed the results and commented on the manuscript.

ADDITIONAL INFORMATION

Supplementary Information accompanies the paper on the *npj 2D Materials and Applications* website (doi:10.1038/s41699-017-0016-4).

Competing interests: The authors declare that they have no competing financial interests.

Change history: A correction to this article has been published and is linked from the HTML version of this article.

REFERENCES

1. Li, X. et al. Graphene and related two-dimensional materials: structure–property relationships for electronics and optoelectronics. *Appl. Phys. Rev.* **4**, 021306 (2017).
2. Li, X. et al. Graphene-on-silicon Schottky junction solar cells. *Adv. Mater.* **22**, 2743–2748 (2010).
3. Urich, A., Unterrainer, K. & Mueller, T. Intrinsic response time of graphene photodetectors. *Nano Lett.* **11**, 2804–2808 (2011).
4. Limmer, T., Feldmann, J. & Da Como, E. Carrier lifetime in exfoliated few-layer graphene determined from intersubband optical transitions. *Phys. Rev. Lett.* **110**, 217406 (2013).
5. Chen, Z. et al. Synergistic effects of plasmonics and electron trapping in graphene short-wave infrared photodetectors with ultrahigh responsivity. *ACS Nano* **11**, 430–437 (2017).
6. Li, X. et al. Anomalous behaviors of graphene transparent conductors in graphene–silicon heterojunction solar cells. *Adv. Energy Mater.* **3**, 1029–1034 (2013).
7. Sun, Z. & Chang, H. Graphene and graphene-like two-dimensional materials in photodetection: mechanisms and methodology. *ACS Nano* **8**, 4133–4156 (2014).
8. Koppens, F. H. L. et al. Photodetectors based on graphene, other two-dimensional materials and hybrid systems. *Nat. Nanotechnol.* **9**, 780–793 (2014).
9. Xia, F., Mueller, T., Lin, Y.-m, Valdes-Garcia, A. & Avouris, P. Ultrafast graphene photodetector. *Nat. Nanotechnol.* **4**, 839–843 (2009).
10. Konstantatos, G. et al. Hybrid graphene-quantum dot phototransistors with ultrahigh gain. *Nat. Nanotechnol.* **7**, 363–368 (2012).
11. Qiao, H. et al. Broadband photodetectors based on graphene–Bi2Te3 heterostructure. *ACS Nano* **9**, 1886–1894 (2015).
12. Lee, Y. et al. High-performance perovskite-graphene hybrid photodetector. *Adv. Mater.* **27**, 41–46 (2015).
13. Wang, Y. et al. Hybrid graphene-perovskite phototransistors with ultrahigh responsivity and gain. *Adv. Opt. Mater* **3**, 1389–1396 (2015).
14. Liu, F. & Kar, S. Quantum carrier reinvestment-induced ultrahigh and broadband photocurrent responses in graphene–silicon junctions. *ACS Nano* **8**, 10270–10279 (2014).
15. Chen, Z. et al. High responsivity, broadband, and fast graphene/silicon photodetector in photoconductor mode. *Adv. Opt. Mater.* **3**, 1207 (2015).
16. Liu, Y. et al. Planar carbon nanotube-graphene hybrid films for high-performance broadband photodetectors. *Nat. Commun.* **6**, 8589 (2015).
17. Roy, K. et al. Graphene-MoS_2 hybrid structures for multifunctional photoresponsive memory devices. *Nat. Nanotechnol* **8**, 826–830 (2013).
18. Zhang, W. et al. Ultrahigh-gain photodetectors based on atomically thin graphene-MoS_2 heterostructures. *Sci. Rep.* **4**, 3826 (2014).
19. Liu, X. et al. Epitaxial ultrathin organic crystals on graphene for high-efficiency phototransistors. *Adv. Mater.* **28**, 5200–5205 (2016).
20. Li, X. & Zhu, H. The graphene–semiconductor Schottky junction. *Phys. Today* **69**, 46–51 (2016).
21. Luo, L. B. et al. A graphene/GaAs near-infrared photodetector enabled by interfacial passivation with fast response and high sensitivity. *J. Mater. Chem. C* **3**, 4723–4728 (2015).
22. Li, X. et al. High detectivity graphene-silicon heterojunction photodetector. *Small* **12**, 595–601 (2016).
23. Zhu, M. et al. Schottky diode characteristics and 1/f noise of high sensitivity reduced graphene oxide/Si heterojunction photodetector. *J. Appl. Phys.* **119**, 124303 (2016).
24. Tsuboi, Y. et al. Enhanced photovoltaic performances of graphene/Si solar cells by insertion of a MoS_2 thin film. *Nanoscale* **7**, 14476–14482 (2015).
25. Song, Y. et al. Role of interfacial oxide in high-efficiency graphene-silicon Schottky barrier solar cells. *Nano Lett.* **15**, 2104–2110 (2015).
26. Li, X., Lv, Z. & Zhu, H. Carbon/silicon heterojunction solar cells: state of the art and prospects. *Adv. Mater.* **27**, 6549–6574 (2015).
27. Liu, Y. et al. High-current-density vertical-tunneling transistors from graphene/highly doped silicon heterostructures. *Adv. Mater.* **28**, 4120–4125 (2016).
28. Sarkar, D. et al. A subthermionic tunnel field-effect transistor with an atomically thin channel. *Nature* **526**, 91–95 (2015).
29. Li, H. et al. From bulk to monolayer MoS_2: evolution of Raman scattering. *Adv. Funct. Mater.* **22**, 1385–1390 (2012).
30. Tao, L. et al. Modification on single-layer graphene induced by low-energy electron-beam irradiation. *J. Phys. Chem. C* **117**, 10079–10085 (2013).
31. Mak, K. F., Lee, C., Hone, J., Shan, J. & Heinz, T. F. Atomically thin MoS_2: a new direct-gap semiconductor. *Phys. Rev. Lett.* **105**, 136805 (2010).
32. Guo, N. et al. Anomalous and highly efficient InAs nanowire phototransistors based on majority carrier transport at room temperature. *Adv. Mater.* **26**, 8203–8209 (2014).
33. Pierucci, D. et al. Band alignment and minigaps in monolayer MoS_2-Graphene van der Waals heterostructures. *Nano Lett.* **16**, 4054–404261 (2016).
34. Sze, S. M. & Ng, K. K. *Physics of semiconductor devices* (Wiley, 2007).
35. Kufer, D. & Konstantatos, G. Photo-FETs: phototransistors enabled by 2D and 0D nanomaterials. *ACS Photon.* **3**, 2197–2210 (2016).
36. OPTEK Technology http://optekinc.com/viewparts.aspx?categoryID=8. Accessed Nov 2016.
37. Ng, K. & Card, H. Asymmetry in the SiO_2 tunneling barriers to electrons and holes. *J. Appl. Phys.* **51**, 2153–2157 (1980).
38. Lu, C.-P., Li, G., Watanabe, K., Taniguchi, T. & Andrei, E. Y. MoS_2: choice substrate for accessing and tuning the electronic properties of graphene. *Phys. Rev. Lett.* **113**, 156804 (2014).
39. Gong, C. et al. Band alignment of two-dimensional transition metal dichalcogenides: application in tunnel field effect transistors. *Appl. Phys. Lett.* **103**, 053513 (2013).

40. Huang, Y. L. et al. Bandgap tunability at single-layer molybdenum disulphide grain boundaries. *Nat. Commun.* **6**, 6298 (2015).
41. Tackeuchi, A., Kuroda, T., Mase, K., Nakata, Y. & Yokoyama, N. Dynamics of carrier tunneling between vertically aligned double quantum dots. *Phys. Rev. B* **62**, 1568 (2000).
42. Jia, G. Y. et al. Excitonic quantum confinement modified optical conductivity of monolayer and few-layered MoS_2. *J. Mater. Chem. C* **4**, 8822–8828 (2016).
43. Hung, K. K., Ko, P. K., Hu, C. & Cheng, Y. C. A unified model for the flicker noise in metal-oxide-semiconductor field-effect transistors. *IEEE Trans. Electron Dev* **37**, 654–665 (1990).
44. Balandin, A. A. Low-frequency 1/f noise in graphene devices. *Nat. Nanotechnol.* **8**, 549–555 (2013).
45. Liu, G., Rumyantsev, S., Shur, M. S. & Balandin, A. A. Origin of 1/f noise in graphene multilayers: surface vs. volume. *Appl. Phys. Lett.* **102**, 093111 (2013).
46. Kayyalha, M. & Chen, Y. P. Observation of reduced 1/f noise in graphene field effect transistors on boron nitride substrates. *Appl. Phys. Lett.* **107**, 113101 (2015).
47. Liu, N. et al. Large-area, transparent, and flexible infrared photodetector fabricated using P-N junctions formed by N-doping chemical vapor deposition grown graphene. *Nano Lett.* **14**, 3702–3708 (2014).
48. De Fazio, D. et al. High responsivity, large-area graphene/MoS_2 flexible photodetectors. *ACS Nano* **10**, 8252–8262 (2016).
49. Tao, L. et al. Centimeter-scale CVD growth of highly crystalline single-layer MoS_2 film with spatial homogeneity and the visualization of grain boundaries. *ACS Appl. Mater. Interfaces* **9**, 12073–12081 (2017).